Vol 18 No 6, June 2009
1674-1056/2009/18(06)/2481-06

Chinese Physics B

© 2009 Chin. Phys. Soc.
and IOP Publishing Ltd

Ab initio prediction on ferrotoroidic and electronic properties of olivine $Li_4MnFeCoNiP_4O_{16}$

Feng Hong-Jian(冯宏剑)† and Liu Fa-Min(刘发民)‡

School of Science, Beijing University of Aeronautics and Astronautics, Beijing 100191, *China*

(Received 25 December 2008; revised manuscript received 12 January 2009)

First-principles calculations predict that olivine $Li_4MnFeCoNiP_4O_{16}$ has a large toroidal moment and ferrimagnetic configuration with a magnetic moment of $1.99\mu_B$ per formula unit. Density functional theory plus U (DFT+U) shows an indirect band gap of 0.65 eV in this hypothetical material. The band gap is not simply related to the electronic conductivity when it is used as cathode material in rechargeable Li-ion batteries. Based on the orbital-resolved density of states for the transition-metal ions in the hypothetical material, Co, Ni and Mn are in the high-spin configuration while Fe is in the low-spin configuration, which leads to a large resulting toroidal moment deriving from the Co and Ni ions. The spin configuration of the transition-metal ions in the system breaks the space- and time-inversion symmetry and leads to the magnetoelectric property simultaneously. The ferrotoroidic domain, the fourth form of ferroic, is observed in this new material, as in the case of $LiCoPO_4$ reported recently.

Keywords: ferrotoroidic, density functional theory, density of states, $Li_4MnFeCoNiP_4O_{16}$
PACC: 7115, 7510,7780

1. Introduction

Ferrotoroidic (FTO) domains have been observed recently in olivine $LiCoPO_4$ using second harmonic generation (SHG), which are independent of the antiferromagnetic (AFM) domains.[1] The ordered arrangement of magnetic vortices is found to be the fourth form of ferroic order, which is currently debated whether to be included or not.[2,3] The well-known three forms of ferroic are ferromagnetism, ferroelectricity, and ferroelasticity. This fourth form of ferroic is named as ferrotoroidicity corresponding to the former three forms, which have been well established and investigated extensively. A ferrotoroidic moment is generated by a vortex of magnetic moment, which is asymmetric under the reversal of time and space. The time- and space-asymmetric property relates ferrotoroidic materials deeply to the multiferroic materials, in which ferromagnetic property violates time reversal symmetry and ferroelectric property violates spatial inversion symmetry. Previously we have investigated a series of multiferroic perovskite materials such as $BiFeO_3$ using a first-principles calculation.[4−7] ABO_3 perovskite materials have been studied intensively for decades due to their simple structure within density functional theory (DFT).[8,9] FTO materials will shed light on the design of new magnetoelectric multiferroic materials.

In olivine $LiCoPO_4$, the Co^{2+} ions are located at positions (1/4+ϵ, 1/4, $-\delta$), where ϵ and δ denote the small displacements according to the mmm symmetry. The four nearest Co^{2+} ions are arranged antiferromagnetically along the y axis and have two different toroidic moments due to the rotation of spins by $\phi = 4.6°$ away from the y axis.[10] The two toroidal moments are opposite in direction and not equal in value, leading to the ferrotoroidic property. If the Co^{2+} sites are substituted by different transition metal ions such as Mn, Fe, and Ni ions, a large resulting toroidal moment and further an excellent ferrotoroidicity would be expected due to the complicated exchange interactions of the different magnetic ions. Magnetism can be improved by substituting transition-metal ions by another one such as in the case of Bi_2FeCrO_6 and Bi_2FeTiO_6.[4,11] In this paper, we partially substitute Co in olivine $LiCoPO_4$ with Mn, Fe, and Ni ions to form $Li_4MnFeCoNiP_4O_{16}$, which can be prepared through conventional solid-state reaction in an oxygen environment experimentally and expected to have significant magnetoelectric coupling effect and the potential to be used as cathode materials for Li-ion rechargeable batteries. In order to

†E-mail: fenghongjian@gmail.com
‡E-mail: fmliu@buaa.edu.cn

gain insight into this predicted material, we have investigated the electronic and magnetic properties using first-principles calculations. The remainder of this article is organized as follows: in Section 2, we present the computational details of our calculations. In Section 3, we report the calculated results and discussion. In Section 4, the conclusions based on our calculations are given.

2. Computational details

Calculations in this work have been done by using the Quantum-ESPRESSO package.[12] Our DFT computations follow the method previously reported in Refs.[4]–[7]. We used a plane-wave pseudopotential with the Perdew–Burke–Ernzerhof (PBE) exchange correlation functional to describe the electron-ion interaction. A plane-wave basis set with kinetic energy cut-off of 40 Ry was employed. Li $2s$, Mn $3s$, $3p$ and $3d$ electrons, Fe $3s$, $3p$ and $3d$ electrons, Co $3s$, $3p$ and $3d$ electrons, Ni $3s$, $3p$ and $3d$ electrons, P $3s$ and $3p$ electrons, and O $2s$ and O $2p$ electrons have been treated as in valence states. A larger cut-off of 300 Ry was used for the charge density, which included the augmentation charges required by the use of ultrasoft pseudopotentials. We used up to $6 \times 7 \times 8$ grids of special k points in total energy calculation, and $8 \times 9 \times 10$ grids of special k points were used for the density of states (DOS) calculation. The initial lattice constants and the atomic positions were taken from Ref.[13]. Then, full structural relaxations were performed by minimization of the Hellman–Feynman forces within a convergence threshold of 10^{-3} Ry/Bohr. The transition-metal ions have been arranged differently to find a favorable structure with minimal energy. Consequently, the stable structure was reached and constructed by XCrySDen as shown in Fig.1.[14] Collinear spin configurations

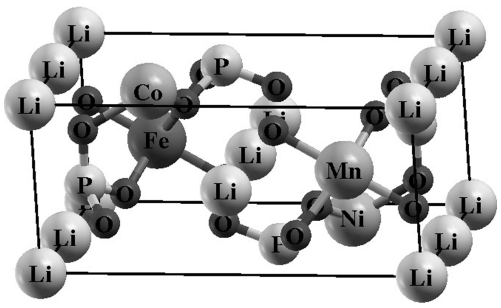


Fig.1. Crystal structures of $Li_4MnFeCoNiP_4O_{16}$ constructed by XCrySDen (Ref.[14]).

have been used to construct the different AFM orders. A Hubbard-like term U was introduced to treat the transition-metal ions, also known as DFT+U. The DFT+U method combines the high efficiency of LDA/GGA and an explicit treatment of correlation with a Hubbard-type model for a subset of states in the system.[15] In the present work, U takes the values 3.92, 3.71, 5.05, and 5.26 for Mn, Fe, Co, and Ni, respectively.[16]

3. Results and discussion

It is known that LiMPO$_4$ (M=Mn, Fe, Co, and Ni) has an orthorhombic cell, which contains four formula units, 28 atoms: 4 lithium, 4M, 4 phosphor, and 16 oxygen atoms. Phosphor ions are tetrahedrally coordinated to oxygen, where M and lithium ions occupy the centers of distorted oxygen octahedral with space group Pnma. The initial lattice parameters and atomic positions are taken from Ref.[11], and we put the Mn, Fe, Co, and Ni ions on the 4M sites with different arrangements. The same atomic species tend to form clusters, and the segregation of Co in LiCoPO$_4$ preclude the homogeneous toroidal moments in the crystal. That is the reason why we substitute Mn, Fe, and Ni in the parent material to prevent the segregation of Co and form an expected large homogeneous toroidal moment. The stable structure under the condition of minimal total energy is shown in Fig.1. Mn and Fe occupy the atomic sites having large toroidal radius, while Co and Ni occupy the atomic sites with smaller toroidal radius. Next, the lattice parameters and atomic positions are fully relaxed. The relaxed lattice parameters and Wyckoff positions are shown in Table 1. The lattice parameters are decreased by 5% as compared with the value of LiFePO$_4$ due to the mixing of different transition-metal ions. With the exception of O_3 atoms, all the other atoms remain fixed in the y direction and move slightly in the x and z directions. We suggest that the fixed positions in the y direction are caused by the exchange interaction of the nearest-neighbor transition-metal ions along the y direction.

We then turn to the spin configuration corresponding to the lowest energy of the hypothetical material. The spin configurations are constructed as no spin, ferromagnetic, and four antiferromagnetic (AFM) configurations (denoted as NM, FM, AFM1, AFM2, AFM3 and AFM4, respectively.). The AFM

Table 1. Relaxed lattice parameters and Wyckoff positions (1 Å = 0.1 nm).

a/Å	b/Å	c/Å	V/Å^3	Wyckoff positions			
9.7570	5.7202	4.5219	252.3762	Li	–0.0003	–0.0003	0.0000
				Mn	0.7767	0.2500	0.5182
				Fe	0.2214	0.7500	0.4788
				Co	0.2752	0.2500	0.9848
				Ni	0.7249	0.7500	0.0140
				P	0.0983	0.2500	0.4232
				O1	0.1025	0.2500	0.7545
				O2	0.4512	0.2500	0.1979
				O3	0.1727	0.0418	0.2725

configurations are shown in Table 2 in detail, and the four atomic sites in different AFM configurations are occupied anticlockwise by Co, Mn, Ni, and Fe, and the y axis is taken to be the positive spin direction. The differences between the total energy of the NM, AFM1, AFM2, AFM3, and AFM4 configurations and their respective total energy in the FM configuration are shown also in Table 2. One can see that the NM configuration has the highest total energy and is the most unstable configuration. The AFM2 is the optimum magnetic configuration. A resulting magnetic moment of 1.99 μ_B is obtained from the calculation, which is related closely to the exchange interaction of the four transition-metal ions.

Table 2. AFM magnetic configuration and calculated differences in total energy (ΔE) in the NM, AFM1, AFM2, AFM3, and AFM4 configurations relative to its total energy in the FM configuration in units of eV/formula unit. The four atomic sites to AFM configuration are Co, Ni, Mn, and Fe respectively. The y axis is taken to be the positive direction of the arrow.

	AFM1	AFM2	AFM3	AFM4	NM
magnetic configuration	↑↑↓↓	↑↓↑↓	↓↓↑↑	↓↑↓↑	
ΔE	–0.02	–0.08	–0.05	–0.07	1.35

A current density distribution of $j_m(r)$ should bring about a toroidal moment T_m defined as

$$T_m = \frac{1}{10c}\int [r(r\cdot j) - 2r^2 j]\mathrm{d}^3 r, \tag{1}$$

where c denotes the speed of light in vacuum. Equation (1) emerges from the multiple expansion of an arbitrary localized current distribution.[3] When this toroidal moment is placed in a specific electromagnetic field, it couples to the curl of the magnetic field such that a toroidal moment which is parallel to the curl of the magnetic field has the lowest energy. Moreover, the toroidal moment can be decomposed into the longitudinal and transverse parts. The former does not contribute to the toroidal moment,[3] while the transverse part can be expressed as the curl of the magnetization density $\mu(r)$:

$$j\perp(r) = c\nabla \times \mu(r). \tag{2}$$

Therefore, the toroidal moment can be given by

$$T_m = \frac{1}{2}\int r \times \mu(r)\mathrm{d}^3 r, \tag{3}$$

in terms of the magnetization denstiy. This form depends strongly on the selection of the unit cell used in the calculation, and cannot be applied directly to the periodic bulk system. In Ref.[17], a localized magnetic moment m_α at sites r_α was introduced to represent the magnetization density

$$\mu(r) = \sum_\alpha m_\alpha \delta(r - r_\alpha). \tag{4}$$

Consequently, the toroidal moment can be obtained

$$T_m = \frac{1}{2}\sum_\alpha r_\alpha \times m_\alpha. \tag{5}$$

This form can be used to evaluate the toroidal moment in periodic bulk material.

In order to analyze the difference between electronic properties caused by the doping effect with

different transition-metal ions and the deviation of atomic positions from the experimental value of $LiFePO_4$, we take the experimental value of $LiFePO_4$ as the reference configuration (fixed structure). The total DOS using DFT and DFT+U for the fixed and relaxed structures are shown in Fig.2. From the DOS it is clear that the manifold states near the Fermi level are mainly attributed to the transition-metal ions. It can be seen that DFT predicts a half-metal behavior for the fixed structure, in which there is only a complete spin polarization of electrons at the Fermi level. DFT also predicts a metal behavior for the relaxed structure, which is not shown in Fig.2. The strong localization of 3d-electrons of this transition-metal leads to the states passing through the Fermi energy, and further to the half-metal characteristic. The strong correlation of these 3d-electrons are well described by employing the DFT+U, and indirect band gap of ∼1.25 eV and ∼0.65 eV are found in the fixed and relaxed structures, respectively, with a proper value of U selected. After relaxation, the lattice parameters are decreased significantly, which are related closely to the narrow band gap. Apparently, one can see that the relaxed structure will have a larger net toroidal moment due to the noticeable difference between the toroidal moments in the clockwise and anticlockwise directions and a relative good conduction property in terms of the smaller band gap.

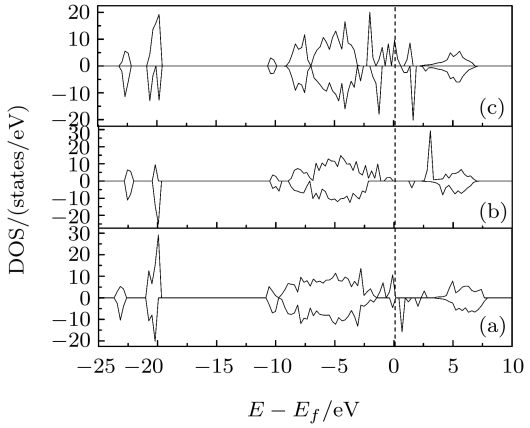


Fig.2. Total DOS of $Li_4MnFeCoNiP_4O_{16}$ after and before relaxation (a) within DFT+U (b), and DFT (c).

In Fig.3 we present the DFT+U band structure for the relaxed structure, taking into account the majority spin and minority spin. It can be seen that it is a semiconductor with an indirect band gap ∼0.65 eV. The valence band top and conduction band bottom lie, respectively, at S and Γ points of the first Brillouin zone. This suggests that the electronic conduction performance of this new material is not very good. A large band gap will lead to a very small number of intrinsically generated electrons or holes when it is used as the cathode material for Li-ion rechargeable batteries, and the band gap will not play a significant role in setting the concentration of conduction electrons or holes. It is likely that the key electrons involved in transport in the predicted material are not delocalized electrons, but localized small polarons, and the mobility is determined by their hopping rate.[18,19] On the other hand, an excellent magnetoelectric effect can be achieved by the insulating property, in which the current leakage is partly precluded. Moreover, from the band dispersion, the valence bands are very dense with little dispersion, while the conduction bands have distinctive dispersions, and these dispersive conduction bands are around 3 eV above the Fermi energy. The conduction bands are composed of antibonding states associated with P–O , M (M=Mn, Fe, Co, and Ni)–O states, and Li 2s states. These states are in the lower-energy region as compared with the LiMPO$_4$ (M=Mn, Fe, Co, and Ni) materials.[20] Hence they provide the possibility of high electron mobility due to their quasi-particle property under lower voltage conditions.

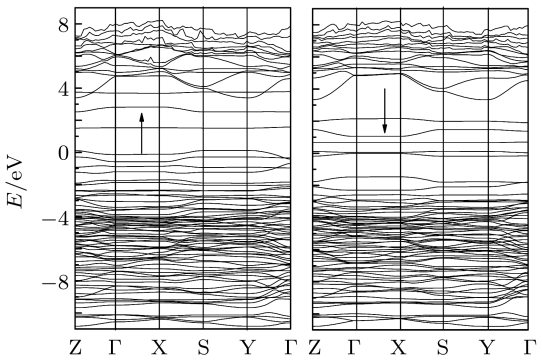


Fig.3. Electronic band structure of $Li_4MnFeCoNiP_4O_{16}$ for the majority-spin and minority-spin states after relaxation. The dotted line indicates the Fermi energy.

Under the distorted oxygen octahedra crystal field, the 3d states of the transition-metal ions can be split into two groups: lower lying t_{2g} states, and higher lying e_g states. In $LiFePO_4$, Fe exists in Fe^{2+} states with $t_{2g}^3(\uparrow)t_{2g}^1(\downarrow)e_g^2(\uparrow)$ since the crystal splitting is smaller than the exchange splitting in this case. And Li and P take the valence states of Li^+ and P^{5+} in the material, respectively. There are a total of four transition-metal ions in this hypothetical structure,

which will definitely exhibit a more complicated magnetic behavior due to the exchange interaction among the four different transition-metal ions. Therefore, all the other cations will exhibit complex valence states to balance the charges in the material.

We report the orbital-resolved DOS for Co, and Ni in Figs.4 and 5 respectively. The t_{2g} and e_g states are decomposed into the d_{xy}, d_{yz}, d_{xz}, d_{z^2}, and $d_{x^2-y^2}$ orbitals respectively. Apparently, Co and Ni ions are all in the high spin configuration as all the majority spin and minority spin are occupied in Co and Ni respectively. Therefore, unlike what we expected in the previous sections, these two atomic sites generated a large toroidal moment. The majority of t_{2g} spin states in Co are well below the Fermi energy, and make the exchange splitting energy of 4.5 eV larger than the crystal-field splitting energy. The electron mobility in Co is partly inhibited by the large exchange splitting energy. There are a small amount of spin states in Ni, occupied and unoccupied states, positioned near the Fermi energy. This leads to a relative smaller exchange splitting as compared with Co. The electron mobility can be induced in Ni in this hypothetical material. Ni will play an important role in the conduction property in the new system.

Similar to Co and Ni, Mn also has a high-spin configuration, while to our surprise all the spin states of Fe, including majority and minority spin states, unlike what we expected in previous sections, are

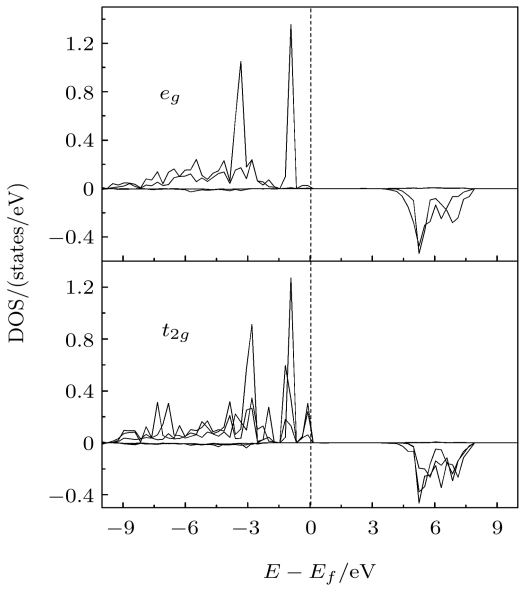


Fig.4. Orbital-resolved DOS for Co t_{2g} and e_g states, decomposing into d_{xy}, d_{yz}, d_{xz}, d_{z^2}, and $d_{x^2-y^2}$ orbitals respectively. Majority-spin states are shown in the upper portions and minority-spin states in the lower portions in all panels. The Fermi level is set to zero.

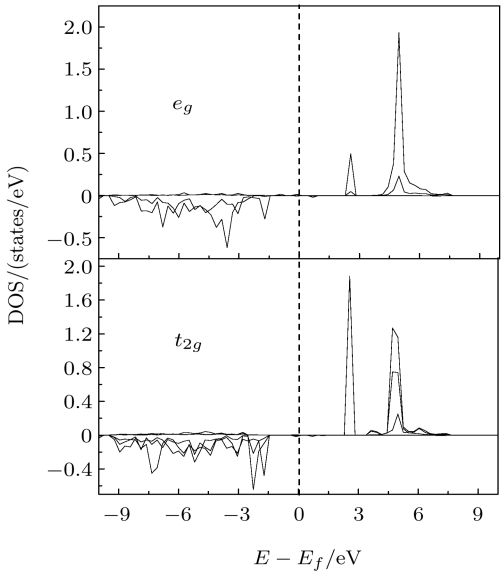


Fig.5. Orbital-resolved DOS for Ni t_{2g} and e_g states, decomposing into d_{xy}, d_{yz}, d_{xz}, d_{z^2}, and $d_{x^2-y^2}$ orbitals respectively. Majority-spin states are shown in the upper portions and minority-spin states in the lower portions in all panels. The Fermi level is set to zero.

all filled, leading to a low-spin configuration. The orbital-resolved DOS for Fe is shown in Fig.6. Although there are a small amount of unoccupied minority spin states in the t_{2g} group, almost all the majority and minority spin states in the five orbitals are filled. This makes the oxidation states and spin configuration more complicated in this new system than in the $LiMPO_4$ material. The excess electrons in the majority spin are mainly migrated from the nearest neighbor (Ni and Co ions) due to the magnetic exchange interaction. There is also electron migration in the Mn caused by Co ions due to the complex interactions among the nearest-neighbor transition-metal ions. The high-spin configurations of Co and Ni are also caused by the same mechanism. The balance of magnetic exchange interactions results in the magnetic moment of 1.99 μ_B per formula unit along the y direction. The toroidal moment caused by the Mn and Fe sites will be decreased significantly to zero. Hence, the resulting toroidal moment is mainly contributed by the anticlockwise direction from the Co and Ni sites. In this case the resultant toroidal moment can be written as:

$$T_m = -\frac{1}{2} r_2 \times S_{\mathrm{Ni+Co}}, \tag{6}$$

where the negative sign indicates the anticlockwise direction, and $S_{\mathrm{Ni+Co}}$ denotes the magnetic moment in Co and Ni ions.

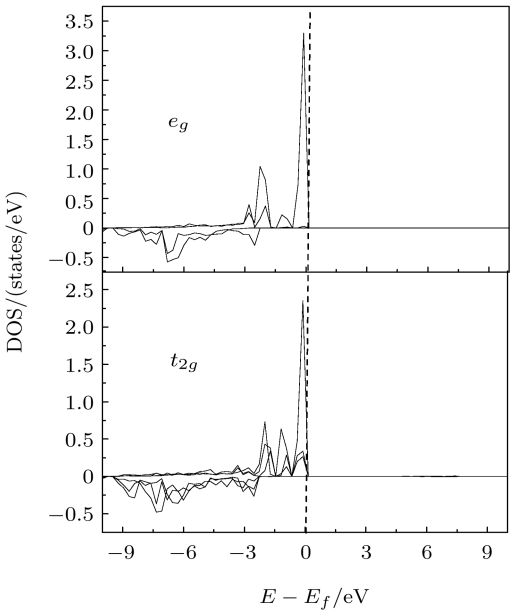


Fig.6. Orbital-resolved DOS for Fe t_{2g} and e_g states, decomposing into d_{xy}, d_{yz}, d_{xz}, d_{z^2}, and $d_{x^2-y^2}$ orbitals respectively. Majority-spin states are shown in the upper portions and minority-spin states in the lower portions in all panels. The Fermi level is set to zero.

In the fixed structure, all the ions are in the high-spin configuration with the exception of Ni ions. Majority spin and minority spin electrons of Ni are all filled in the fixed structure as those of Fe in the relaxed structure. Therefore, in the fixed structure the clockwise toroidal moment caused by the Co and Ni ions disappears, while the resultant moment is mainly attributed to the Mn and Fe ions. It can be seen that the resultant toroidal moment is strongly affected by the lattice parameters and internal atomic coordinates, which can be controlled experimentally by the doping concentration of the transition-metal ions and other experimental conditions.

4. Conclusion

Motivated by the ferrotoroidic domains observed in $LiCoPO_4$, we proposed a new material formed partially substituting Co by Mn, Fe, and Ni ions. Based on an investigation of the structural relaxation and spin configuration, first-principles calculations show that the resulting toroidal moment, derived mainly from Co and Ni ions, is noticeable due to the low-spin configuration of Fe in the relaxed structure. The low-spin configuration of Fe also shows that there is high electronic migration among the metal ions. Moreover, Ni becomes low-spin configuration as the experimental lattice parameters are applied in the calculation, and the direction of magnetic torque in a unit cell is altered in this case. This suggests that the direction of the toroidal moment, and further the ferrotoroidic domains, can be changed by the structural parameters. Therefore, this material is expected to have excellent ferrotoroidictiy, and it can be used as multiferroic material in terms of its magnetoelectric effect due to the simultaneous broken time and space reversal symmetry. Calculations using DFT+U reveal that the indirect band gap is ∼0.65 eV. When this multiferroic material is used as cathode material in rechargeable Li-ion batteries, the electronic conductivity is not simply related to the indirect band gap, but also to the localized small polarons and polaron conduction.

References

[1] Van Aken B B, Rivera J P, Schmid H and Fiebig M 2008 *Nature* **449** 702

[2] Fiebig M 2005 *J. Phys.* D: *Appl. Phys.* **38** R123

[3] Dubovik V M and Tugushev V V 1990 *Phys. Rep.* **187** 145

[4] Feng H J and Liu F M 2008 *Phys. Lett.* A **372** 1904

[5] Feng H J and Liu F M 2008 *Chin. Phys. Lett.* **25** 671

[6] Feng H J and Liu F M 2008 *Chin. Phys.* B **17** 1874

[7] Feng H J and Liu F M 2009 *Chin. Phys.* B **18** 1574

[8] Meng X, Xu X G, Liu W, Sun Y and Cheng G 2004 *Acta Phys. Sin.* **53** 3873 (in Chinese)

[9] Wang Y X, Zhong W L, Wang C L and Zhang P L 2001 *Acta Phys. Sin.* **51** 171 (in Chinese)

[10] Vaknin D, Zarestky J L, Millier L L, Rivera J P and Schid H 2002 *Phys. Rev.* B **65** 224414

[11] Baettig P and Spaldin N A 2005 *Appl. Phys. Lett.* **86** 012505

[12] Baroni S, Corso A D, Gironcoli S, Giannozzi P, Cavazzoni C, Ballabio G, *et al* http://www.pwscf.org/.

[13] Streltsov V A, Belokoneva E L, Tsirelson V G and Hansen N K 1993 *Acta Crystallogr.* Sect. B: *Struct. Sci.* **49** 147

[14] Kokalj A 1999 *J. Mol. Graphics Model.* **17** 176

[15] Liechtenstein A I, Anisimov V I and Zaanen J 1995 *Phys. Rev.* B **52** R5467

[16] Zhou F, Cococcioni M, Marianetti C A, Morgan D and Ceder G 2004 *Phys. Rev.* B **70** 235121

[17] Ederer C and Spaldin N A 2007 *Phys. Rev.* B **76** 214404

[18] Maxisch T, Zhou F and Ceder G 2006 *Phys. Rev.* B **73** 104301

[19] Zhou F, Kang K, Maxisch T, Ceder G and Morgan D 2004 *Solid State Commun.* **132** 181

[20] Tang P and Holzwarth N A W 2003 *Phys. Rev.* B **68** 165107